Title

Optimizing an Antioxidant TEMPO Copolymer for Reactive Oxygen Species Scavenging and Anti-Inflammatory Effects in Vivo



Journal

Bioconjugate Chemistry, 32(5)

ISSN

1043-1802

Authors

DeJulius, Carlisle R

Dollinger, Bryan R

Kavanaugh, Taylor E

et al.

Publication Date

2021-05-19

DOI

10.1021/acs.bioconjchem.1c00081

Peer reviewed

HHS Public Access

Author manuscript

*Bioconjug Chem*. Author manuscript; available in PMC 2022 May 19.

Published in final edited form as:

*Bioconjug Chem*. 2021 May 19; 32(5): 928–941. doi:10.1021/acs.bioconjchem.1c00081.

# Optimizing an Antioxidant TEMPO Copolymer for Reactive Oxygen Species Scavenging and Anti-Inflammatory Effects *in Vivo*

**Carlisle R. DeJulius**,
Department of Biomedical Engineering, Vanderbilt University, Nashville, Tennessee 37232, United States

**Bryan R. Dollinger**,
Department of Biomedical Engineering, Vanderbilt University, Nashville, Tennessee 37232, United States

**Taylor E. Kavanaugh**,
Department of Biomedical Engineering, Vanderbilt University, Nashville, Tennessee 37232, United States

**Eric Dailing**,
Department of Biomedical Engineering, Vanderbilt University, Nashville, Tennessee 37232, United States

**Fang Yu**,
Department of Biomedical Engineering, Vanderbilt University, Nashville, Tennessee 37232, United States

**Shubham Gulati**,
Department of Biomedical Engineering, Vanderbilt University, Nashville, Tennessee 37232, United States

**Angelo Miskalis**,
Department of Biomedical Engineering, Vanderbilt University, Nashville, Tennessee 37232, United States

**Caiyun Zhang**,
Department of Biomedical Engineering, Vanderbilt University, Nashville, Tennessee 37232, United States; Anhui University of Chinese Medicine, Hefei, Anhui 230000, China

**Jashim Uddin**,

**Corresponding Author**, Craig L. Duvall – Phone: 615-322-3598; craig.duvall@vanderbilt.edu; Fax: 615-343-7919.

ASSOCIATED CONTENT

Supporting Information

The Supporting Information is available free of charge at https://pubs.acs.org/doi/10.1021/acs.bioconjchem.1c00081.

$^{1}H$ and $^{19}F$ NMR scans of each polymer in the series, logP quantification, ESR spectra, dose-finding study for air pouch model, and $t_{1/2}$ and biodistribution quantification (PDF)

The authors declare no competing financial interest.

Department of Biochemistry, Vanderbilt University School of Medicine, Nashville, Tennessee 37232, United States

**Sergey Dikalov**,
Vanderbilt University Medical Center, Nashville, Tennessee 37232, United States

**Craig L. Duvall**
Department of Biomedical Engineering, Vanderbilt University, Nashville, Tennessee 37232, United States

## Abstract

Oxidative stress is broadly implicated in chronic, inflammatory diseases because it causes protein and lipid damage, cell death, and stimulation of inflammatory signaling. Supplementation of innate antioxidant mechanisms with drugs such as the superoxide dismutase (SOD) mimetic compound 2,2,6,6-tetramethylpiperidin-1-oxyl (TEMPO) is a promising strategy for reducing oxidative stress-driven pathologies. TEMPO is inexpensive to produce and has strong antioxidant activity, but it is limited as a drug due to rapid clearance from the body. It is also challenging to encapsulate into micellar nanoparticles or polymer microparticles, because it is a small, water soluble molecule that does not efficiently load into hydrophobic carrier systems. In this work, we pursued a polymeric form of TEMPO [poly(TEMPO)] to increase its molecular weight with the goal of improving *in vivo* bioavailability. High density of TEMPO on the poly(TEMPO) backbone limited water solubility and bioactivity of the product, a challenge that was overcome by tuning the density of TEMPO in the polymer by copolymerization with the hydrophilic monomer dimethylacrylamide (DMA). Using this strategy, we formed a series of poly(DMA-*co*-TEMPO) random copolymers. An optimal composition of 40 mol % TEMPO/60 mol % DMA was identified for water solubility and $O_2^{\bullet-}$ scavenging *in vitro*. In an air pouch model of acute local inflammation, the optimized copolymer outperformed both the free drug and a 100% poly(TEMPO) formulation in $O_2^{\bullet-}$ scavenging, retention, and reduction of TNF$\alpha$ levels. Additionally, the optimized copolymer reduced ROS levels after systemic injection in a footpad model of inflammation. These results demonstrate the benefit of polymerizing TEMPO for *in vivo* efficacy and could lead to a useful antioxidant polymer formulation for next-generation anti-inflammatory treatments.

## Graphical Abstract

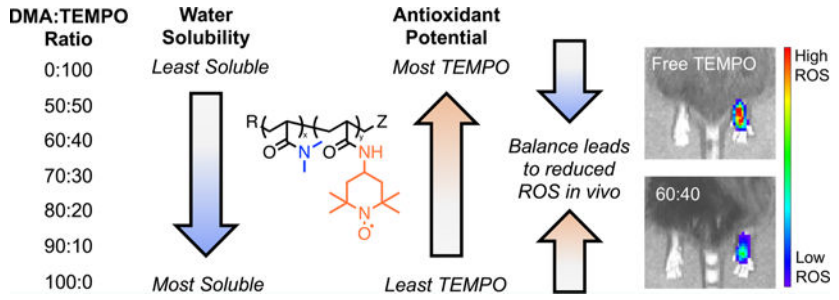

## INTRODUCTION

Reactive oxygen species (ROS) encompass oxidizing compounds with oxygen as the REDOX center and include free radicals such as superoxide anion ($O_2^{\bullet -}$) and hydroxyl radical ($OH^{\bullet}$), as well as nonradical species such as hydrogen peroxide ($H_2O_2$) and hypochlorite ion ($OCl^-$).[1–3] ROS have important biological functions, such as in host defense and cell signaling, when normal homeostasis is maintained.[1,2] Oxidative stress occurs when ROS levels overwhelm cells' ability to neutralize them through natural antioxidant mechanisms.[4] Oxidative stress is implicated in a wide variety of chronic inflammatory diseases, including rheumatoid arthritis (RA), cancer, diabetes, and atherosclerosis.[5–8] The mechanism of ROS in exacerbating inflammation involves multifaceted, interrelated factors including direct biomolecule damage, upregulation of nuclear factor κ-light-chain-enhancer of activated B cells (NF-κB) signaling, and cell death.[1,3,9,10]

Cells possess innate antioxidant defenses to maintain ROS homeostasis, including the enzymes superoxide dismutase (SOD), catalase (CAT), glutathione peroxidase (GPX), and peroxiredoxins, in addition to the chemical scavengers vitamins A, C, and E and glutathione.[11] Of these, SOD plays a major role in antioxidant activity by catalyzing the conversion of $O_2^{\bullet -}$ to the less reactive $H_2O_2$,[12] which is in turn converted to $O_2$ and $H_2O$ by CAT. Because of its key function in scavenging $O_2^{\bullet -}$ and maintaining normal cellular function, SOD has been investigated preclinically as a therapy for ischemic brain[13] and myocardial[14] injury, liver damage,[15] and lung metastasis.[16] In clinical trials, SOD therapy has shown the most promise for treatment of skin disorders including radiation-induced fibrosis and dermatitis, vitiligo, and melasma. SOD has also been investigated for age-related macular degeneration, vascular reactivity to inflammation, myocardial reperfusion injury, and sleep apnea. However, SOD suffers from a short half-life ($t_{1/2}$) *in vivo*, an inability to cross cell membranes, and its need to be produced by recombinant techniques, all of which limit its therapeutic usefulness and practicality.[17] One strategy to overcome these challenges is to modify SOD, such as by conjugation to targeting antibodies,[18,19] polymeric electrostatic coupling,[20] and direct polymer conjugation.[21,22]

Another strategy to recapitulate SOD activity is to use small molecule mimetics of SOD for $O_2^{\bullet -}$ scavenging. These alternatives tend to be less expensive and more synthetically versatile. The small molecule 2,2,6,6-tetramethylpiperidine-1-oxyl (TEMPO) has garnered interest as a SOD mimetic due to its catalytically active, stable aminoxyl radical. Clinically, a hydroxy-functionalized TEMPO derivative (Tempol) has been tested for its ability to prevent radiation-induced toxicities and treat cardiovascular disease. Preclinically, targeting of TEMPO to mitochondria (MitoTEMPO[23]) has demonstrated efficacy in diabetic cardiomyopathy[24] and hypertension,[25] among other conditions.[26–28]

In this work, we sought a facile strategy to polymerize TEMPO while maintaining its bioactivity. Previous work on TEMPO polymers focuses on integration of poly(TEMPO) homopolymers into nanoparticles and hydrogels.[29–31] Here, we generated a series of random copolymers of TEMPO and a hydrophilic spacer monomer with the goal of determining an optimal TEMPO backbone density to maintain water solubility while maximizing radical

scavenging potential. The effect of polymer composition was screened *in vitro* to determine this optimal ratio, which was then tested in two *in vivo* models for ROS scavenging and anti-inflammatory effects.

## RESULTS AND DISCUSSION

### Generating a Series of DMA-*co*-TEMPO Polymers with Precise Control of TEMPO Content.

To tune the water solubility of TEMPO copolymers, TEMPO was copolymerized in varying ratios with the hydrophilic spacer monomer *N,N*-dimethylacrylamide (DMA). A series of DMA-*co*-TEMPO copolymers with TEMPO content ranging from 0% to 100% was synthesized according to the two-step synthesis scheme shown in Figure 1A. First, DMA monomer and amine-reactive pentafluorophenyl acrylate (PFPA) monomer were copolymerized via reversible addition–fragmentation chain transfer (RAFT) polymerization at varied monomer feeds (0, 50, 60, 70, 80, 90, 100 mol % DMA) to control the random copolymer composition (Supporting Information (SI) Figures S1–7, A–B). After RAFT polymerization, amino-TEMPO was conjugated through the pentafluorophenyl (PFP) ester onto the polymer backbone. The removal of PFP was confirmed by $^{19}$F NMR (Figure 1B and SI Figures S1–7, C–E). Broad $^{19}$F signal represents polymerized PFPA, with sharp shifted peaks representing a small fraction of spontaneously hydrolyzed PFP ($\delta$ = −163.75, −164.98, and −170.62 ppm).[32] The series of polymers is henceforth defined based on TEMPO target content: 0T indicates 0 mol % TEMPO and 100 mol % DMA, 40T indicates targeting of 40 mol % TEMPO and 60 mol % DMA, and so forth.

The polymers were characterized for molecular weight (MW) and polydispersity by GPC. The light scattering detector traces demonstrate polymers with unimodal peaks and progressively higher MW as TEMPO content increases (Figure 2A). A summary of the characterization of the polymers is listed in Figure 2B. For each targeted polymer composition, the ratio of DMA:PFPA was very close to the target, and dispersity values were all <1.3, reflecting the precision of RAFT polymerization. Number- and weight-average MW were both found to increase with increasing TEMPO mol %. Of note, the 100% TEMPO polymer has a lower MW than other compositions because the PFPA monomers did not homopolymerize as efficiently as the copolymer formulations (~85% vs >95% conversion, respectively), resulting in a shorter chain length.

Reverse phase HPLC was used to determine the relative polarity of the polymers. By exposing the column to a gradient with progressively more nonpolar mobile phase, elution time can be used as an indirect measure of polarity, with earlier elution indicating higher polarity and vice versa. As TEMPO content of the series increased, elution time increased, indicating that TEMPO content increases hydrophobicity of the polymers (Figure 2C). This data agreed with octanol/water partition experiments, in which the partition coefficient (logP) trended upward as TEMPO density increased (SI Figure S8A). 40T represented a threshold above which the polymers aggregated in aqueous solution instead of dissolving (SI Figure S8B–C). These data indicate that copolymer water solubility is dependent on the ratio of DMA:TEMPO; higher TEMPO density on the polymers makes them less water-soluble, in line with previous reports that TEMPO homopolymers are insoluble in water at physiological pH.[33,34]

Electron spin resonance (ESR) can detect stable radicals such as the aminoxyl radical of TEMPO with high sensitivity and specificity;[35,36] it was therefore utilized to confirm successful conjugation of active TEMPO to the polymer backbone. As expected, with increasing TEMPO content, the intensity of the ESR signal increased (Figure 2D). Additionally, the ESR spectra gradually broadened as TEMPO density on the backbone increased, due to the spin–spin interaction of the closely packed radicals[34,37] (SI Figure S9). These data confirm that active TEMPO was incorporated by post-polymerization modification and that the relative TEMPO density on the polymers correlated to the monomer feed of PFPA in the RAFT reaction. Overall, a set of polymers was generated with targeted ratios of DMA:TEMPO ranging from 0:100 to 100:0, to be used to evaluate the optimal TEMPO density for biological activity.

### Optimizing TEMPO Density for *in Vitro* $O_2^{\bullet-}$ Scavenging.

After synthesizing the copolymer library, we set out to determine the effect of TEMPO backbone density on $O_2^{\bullet-}$ scavenging. To first characterize the general reducing potential of these polymers, a commercial ferric reducing antioxidant power (FRAP) assay was used. This assay is based on a colorimetric change upon reduction of iron from the ferric ($Fe^{3+}$) to the ferrous ($Fe^{2+}$) form.[38] By matching the dose of polymers in the assay at 20 $\mu$g, it was demonstrated that the 20T–40T polymers had the highest activity, with intermediate levels for 50T and 10T, and significantly reduced activity for 100T (Figure 3A). In the study of dose-matched TEMPO (170 $\mu$M), the activity of the polymers increases as TEMPO density decreases, indicating that the polymers are more active as they become more water-soluble (Figure 3B), correlating with HPLC polarity analysis and logP measurements.

To more specifically probe $O_2^{\bullet-}$ scavenging, the reduction of ferricytochrome C was utilized. $O_2^{\bullet-}$ was generated by the reaction between xanthine oxidase (XO) and hypoxanthine (HX),[12] with $H_2O_2$ being scavenged by CAT to isolate the effect of $O_2^{\bullet-}$.[39] Similar to the FRAP results, $O_2^{\bullet-}$ scavenging was strongest for 30T and 40T when normalized to polymer mass (20 $\mu$g), with 100T exhibiting no $O_2^{\bullet-}$ scavenging (Figure 3C). When normalized to moles of TEMPO (170 $\mu$M), the scavenging activity increased as the TEMPO mol % was reduced from 100T to 40T. However, there was a plateau with similar scavenging activity between 40 and 10T indicating that the activity of TEMPO was not limited by polymer solubility within this composition range at the concentration tested (Figure 3D). Taken together, these data define the structure–function relationship between TEMPO density on the polymer backbone and its relative bioavailability for $O_2^{\bullet-}$ scavenging. At 100% or even 50% TEMPO, activity is suppressed due to poor water solubility. However, if DMA content is too high (20% or 10% TEMPO), the TEMPO density is too low for optimal activity on a polymer per mass basis. Observations in the TEMPO dose-matched assays further confirm that 40 mol % TEMPO density represents a critical threshold above which relative activity of the TEMPO molecules is suppressed.

To the best of our knowledge, only one other study has investigated the effect of TEMPO density on a polymer backbone for ROS scavenging activity.[40] Yoshitomi et al. conjugated TEMPO to a poly(chloromethylstyrene) (PCMS) backbone via condensation reaction with Tempol at densities ranging from 22% to 93% and coated the resulting polymer onto glass

nanobeads. In this system, the authors found that increased TEMPO density increased the level of $O_2^{\bullet-}$ scavenging, in contrast to our finding that an intermediate level of TEMPO grafting is optimal. However, solubility was not a controllable parameter for their system, as the PCMS backbone rendered all polymers hydrophobic regardless of TEMPO density. Additionally, the formation of a thin coating layer on the glass beads potentially yields better availability of the TEMPO groups, as opposed to the aggregates formed by 100T homopolymer in solution. Therefore, to the best of our knowledge, this is the first demonstration of tuning TEMPO density and subsequent water solubility to optimize radical potential and $O_2^{\bullet-}$ scavenging of unimeric polymers in solution.

We further probed the activity of the polymers in cell-based assays using the ATDC5 chondrogenic cell line. All DMA-*co*-TEMPO copolymers were noncytotoxic up to a dose of 5 mg/mL (SI Figure S10), with all polymers at all doses demonstrating cell viability >90%. Additionally, polymerization of TEMPO, particularly at an intermediate density which maintains polymer solubility while promoting hydrophobic cell surface interactions, promotes cell uptake of the drug. Confocal microscopy on cells treated with Cy5-labeled polymers demonstrates higher uptake for 40T compared to polymers with lower TEMPO backbone densities (Figure 4A). Cells were washed thoroughly before imaging, and extracellular Cy5 fluorescence was quenched with TCEP. To compare directly with small molecule Tempol, a complementary experiment was completed with simple treatment media removal but without washing, because Tempol diffuses out of cells rapidly during washes.[41] Treated cell samples were harvested and scanned by ESR, confirming the increased uptake of 40T compared to other formulations and Tempol (Figure 4B). Though the ESR method does not differentiate between surface-associated and internalized polymer, this did not play an apparent role in the study, as the ESR and microscopy results correlated well among the different polymers groups. Notably, 50T and 100T polymers could not be analyzed for cell uptake due to their formation of large, insoluble aggregates in aqueous solution (SI Figure S8B–C). These observations indicate that the balance of hydrophobic and hydrophilic character is necessary for optimal cell uptake.

The effect of hydrophobicity on cell uptake has been observed for other polymer libraries, including poly(2-oxazoline) (POx) amphiphiles,[42] Pluronics,[43] and alkyl-grafted anionic polymers.[44] For fully water-soluble POx polymers, Luxenhofer et al. found that more hydrophobic polymers exhibited higher levels of cell uptake in MCF7-ADR cells,[42] whereas Batrakova et al. demonstrated that Pluronics with intermediate hydrophobic (poly(propylene oxide)) block lengths were best internalized by bovine brain microvessel endothelial cells.[43] Dailing et al. demonstrated that polymer cell uptake of amphiphiles with varying alkyl side chain density correlated with hydrophobicity up to a threshold point; there was monotonic increase in uptake of the polymers themselves as a function of alkyl length for all alkyl densities tested (10, 30, and 50 mol %), up until polymer solubility was lost (50 mol % density with dodecyl alkyl length).[44] These studies support the idea that copolymers with hydrophilic and hydrophobic monomers can be tuned to modulate cell uptake. Though a detailed examination of uptake mechanism is outside the scope of this study, we speculate that the increased hydrophobic character of the 40% TEMPO polymer allows for increased interaction with the lipids of the cell membrane (supported by the measured logP value of 40T near 0, SI Figure S8A). Luxenhofer et al. also showed that uptake of POx amphiphiles

was significantly inhibited at 4 °C,[42] indicating active endocytosis is required for polymer uptake, which could explain the higher intracellular level of 40T polymer over small molecule Tempol, which enters cells through passive diffusion.[45]

Targeting of antioxidants to specific cell compartments is a complementary area of research. The mitochondria-targeted Tempol MitoTEMPO achieves mitochondrial accumulation superior to untargeted Tempol by conjugation with the lipophilic triphenylphosphonium cation.[23] The mitochondria is a substantial source of intracellular ROS; indeed, MitoTEMPO has demonstrated efficacy in diabetic cardiomyopathy,[24] hypertension,[25] acetaminophen hepatotoxicity,[26] oxalate-induced injury,[27] and renal fibrosis.[28] Intracellular targeting of SOD and CAT have also been investigated. Conjugation of SOD to an antibody against plasmalemmal vesicle-associated protein (Plvap) promotes superoxide scavenging specific to caveolae-derived endosomes, outperforming untargeted SOD to suppress lipopolysaccharide (LPS) signaling.[19] These studies demonstrate that targeting of cellular uptake to specific fates can enhance ROS scavenging mechanisms of antioxidants.

One effect of excessive $O_2^{\bullet-}$ is the induction of cell apoptosis. The mechanisms for $O_2^{\bullet-}$-induced cell death include cytochrome C release from mitochondria and increased activity of caspase, NF-$\kappa$B, and p38 mitogen-activated protein kinase (MAPK).[46,47] To quantify the cell protective effect of DMA-*co*-TEMPO copolymers, we treated ATDC5 cells with 1 mM 3-morpholinosydnonimine (SIN-1), which decomposes to $O_2^{\bullet-}$ and nitric oxide ($NO^{\bullet}$) in aqueous solution.[48] $O_2^{\bullet-}$ and $NO^{\bullet}$ recombine to form peroxynitrite.[49] Tempol can provide cell protection against SIN-1 potentially both by scavenging the $O_2^{\bullet-}$ intermediate and by scavenging peroxynitrite decomposition products.[50] This level of ROS caused ~100% cell death with no scavenger present, but 20 $\mu$g 40T polymer rescued viability to ~49% of the non-ROS treated controls (Figure 4C). The same (weight-matched) dose of 10T, 20T, 30T, and 50T polymers demonstrated less rescue (10–40%), while the homopolymers (100% TEMPO or 100% DMA) showed no rescue at all. In the TEMPO dose-matched scenario (Figure 4D), 170 $\mu$M TEMPO delivered in the soluble polymeric formulations (10–40T) demonstrated 41–52% cell rescue (no significant differences). The relatively insoluble formulations were ineffective at protecting ATDC5 cells from SIN-1, while free Tempol achieved ~85% viability. These functional results demonstrate the benefit of tuning TEMPO density on the polymer backbone for cytoprotection from exogenous $O_2^{\bullet-}$.

Cellular protection from ROS-induced cell death has been demonstrated for a variety of ROS scavenging polymers. The majority of studies have utilized polymers formulated into biomaterials like hydrogels, nano/microparticles, or coatings, as opposed to solubilized unimeric polymers. Work from our group has demonstrated the cell protection properties of poly(propylene sulfide) (PPS), a hydrophobic scavenger of various ROS,[51] but in particular $H_2O_2$, in the form of microparticles and hydrogels.[52–54] Similarly, Wong and colleagues formulated a hydrogel from pullulan, a glycan carbohydrate capable of scavenging ROS,[55] and demonstrated its ability to prevent $H_2O_2$-induced death of mesenchymal stem cells (MSCs).[56] A nanoparticle with TEMPO and phenylboronic acid pinacol ester (PBAP) functionalities also significantly reduced RAW264.7 macrophage apoptosis in response to $H_2O_2$.[30] In an interesting application, Yoshitomi et al. coated a TEMPO homopolymer onto cigarette filters and measured the cytotoxicity of the resulting smoke extract, finding that

ROS scavenging of the filter significantly reduced Caco-2 cell death.[33] However, all of these applications represent integration of the ROS-responsive polymer into a more complex system. The few studies that have investigated free polymers in solution have focused on naturally derived antioxidants. Oligomeric and polymeric procyanidins, a type of flavonoid found in grapes, can protect HepG2 cells from *tert*-butyl hydroperoxide (TBHP)-induced cell death,[57] and seaweed-derived agaro-oligosaccharides rescue liver L-02 cells from cytotoxicity of $H_2O_2$.[58] Our DMA-*co*-TEMPO system provides a simple, readily scalable, and chemically well-defined synthetic polymeric antioxidant that can be readily utilized for parenteral or intravenous (i.v.) delivery, with the 40T composition providing the best antioxidant activity *in vitro*.

### Anti-Inflammatory Effects of Optimized TEMPO Copolymer *in Vivo*.

Scavenging ROS has shown efficacy in many inflammatory disease models, including atherosclerosis,[30] stroke,[59] and diabetic peripheral arterial disease.[53] We utilized the inflammatory compound carrageenan to evaluate the anti-inflammatory effects of 40T using both local and systemic administration. As a local model of inflammation, the dorsal air pouch model was utilized (Figure 5A).[60] A preliminary dose-finding study identified 5 mg/animal as an appropriate dose for the 40T treatment based on tumor necrosis factor $\alpha$ (TNF$\alpha$) levels and polymer retention in the exudate (SI Figure S11). To evaluate our lead candidate 40T polymer, 40T, 100T, and free Tempol were coinjected with carrageenan in the air pouch. TEMPO dose was matched across treatments (8.48 $\mu$mol/animal). After 6 h, polymer retention in the pouch was measured by ESR, demonstrating full clearance of the small molecule Tempol, ~12% retention of 40T, and ~94% retention of 100T (Figure 5B). Additionally, TNF$\alpha$ levels in the pouch exudate were significantly reduced with 40T compared to no treatment and Tempol (Figure 5C). After 24 h, 40T significantly reduced ROS levels in the exudate to baseline levels, with no effect of saline, Tempol, or 100T (Figure 5D). We interpret the stronger anti-inflammatory effect of the polymeric over free small molecule Tempol to be due to the improved retention of the polymer in the air pouch, allowing for extended ROS scavenging and suppression of inflammation. It is interesting to note that the impressive retention of 100T is an effect of its insolubility and aggregation, yielding retention in an inactive form within the air pouch. The inability of this polymer to significantly reduce TNF$\alpha$ or ROS levels despite its excellent retention indicates that optimizing the density of TEMPO on the polymer backbone is crucial for anti-inflammatory activity *in vivo*.

The efficacy of antioxidant therapy in the air pouch model has been investigated by others. Drugs including 10-(6′-plastoquinonyl)decyltriphenylphosphonium bromide (SkQ1), C*ressa cretica* extract, TS-13 (a *tert*-butyl phenol thiosulfonate), and atorvastatin have shown anti-inflammatory effects in this model.[61–64] These results are promising; however, all of these treatment options required prophylactic administration 1 h or 1–10 days (daily) before carrageenan injection to achieve therapeutic efficacy. In contrast, coadministration of our optimized TEMPO copolymer reduced both $O_2^{\bullet-}$ and TNF$\alpha$ levels in the air pouch by ~90% and ~83%, respectively. In another example of coadministration, the novel small molecule 4*b*,9*b*-dihydroxy-6-methoxy-8-(3-oxo-but-1-enyl)-4*b*,9*b*-dihydro-5-oxa-indeno[2,1-$\alpha$]inden-10-one (DMFO) reduced cell infiltration and NO levels in the air pouch. This effect

was found to be due to both direct radical scavenging and activation of nuclear factor erythroid 2-related factor 2 (Nrf2) signaling.[65] These results indicate that stimulation of innate cellular antioxidant mechanisms in combination with direct scavenging could be more effective than scavenging alone.

We were also interested in the capability of our polymers to alleviate inflammation with systemic administration. Preliminary intravital microscopy (IVM) studies with cyanine5 (Cy5)-labeled polymers (200 $\mu$g, i.v.) demonstrated that the distribution $t_{1/2}$ for the water-soluble copolymers (10–40T) trended upward from ~5.8 to ~17.5 min as TEMPO content increased (SI Figure S12A). The $t_{1/2}$ of Tempol has been found to be ~3 min, indicating that polymerization improves systemic circulation.[66] 40T and 30T exhibited similar $t_{1/2}$, though 30T trended toward having higher kidney and lower liver distribution relative to 40T (SI Figure S12B). Based on these studies, a dose of 200 $\mu$g 40T was selected for treatment in the inflammatory footpad model. Tempol and 30T were also injected at a matched TEMPO dose (377 nmol). Carrageenan was injected locally into the footpad of C57/Bl6 mice, and inflammation was allowed to develop for 6 h before treatment. This treatment regimen allows for cyclooxygenase-2 (COX2)-derived prostaglandins to establish high levels of ROS and other inflammatory mediators.[67] Both polymers reduced footpad ROS levels by ~33%, while Tempol had no effect (Figure 6A–B). Notably, a larger mass dose of 30T (~260 $\mu$g vs 200 $\mu$g) was required to achieve this effect than 40T due to its lower TEMPO density. We hypothesize that the circulation time of our polymers allows for improved accumulation and that the larger MW contributes to longer tissue retention in the inflamed footpad over small molecule Tempol. Inflamed tissues encourage passive targeting and retention of therapeutics via the extravasation through leaky vasculature and the subsequent inflammatory cell-mediated sequestration (ELVIS) effect.[68,69] Similar to the enhanced permeation and retention (EPR) effect in tumors, many drugs naturally accumulate in inflammatory tissues, a phenomenon which has been shown to correlate with increasing polymer–drug conjugate molecular weight or nanoparticle packaging.[68–72] The ability for our polymers to reduce ROS levels in this aggressive model where inflammation has developed for 6 h is encouraging for treatment of more established disease.

Antioxidant therapy has been investigated previously in the carrageenan footpad model, with most treatments administered prophylactically (similar to the air pouch model). For example, Chedid et al. demonstrated the ability of vasoactive intestinal peptide (VIP) to reduce cellular ROS production *in vitro* and ameliorate footpad edema *in vivo* when administered 1 day and 1 h prior to carrageenan injection.[73] Similarly, antioxidant fullerenol nanoparticles[74] and *Ficus exasperata* bark extract[75] significantly reduced edema as a prophylactic treatment. These results support systemic antioxidant treatment for aggressively inflammatory conditions. Notably, our polymers were able to reduce ROS after 6 h of inflammation, though we did not measure the functional outcome of edema. Additionally, our effect was seen after i.v. administration as opposed to i.p. or oral administration utilized in other studies.[73–75]

Others have demonstrated the beneficial effects of polymeric TEMPO formulations in oxidative stress-driven diseases. Much of this work has been pursued by the Nagasaki group, who has formulated TEMPO polymers into nanoparticles, hydrogels, and device coatings.

[29,31,33,34,40] These studies have demonstrated the efficacy of TEMPO polymer formulations in cerebral ischemia-reperfusion injury and inflammatory arthritis, among other disease models. Hydrogel and nanoparticle preparations have demonstrated significant improvements in TEMPO retention upon hind paw injection[31] and increased $t_{1/2}$ upon i.v. injection,[29] similar to our finding of improved retention in the air pouch and increased systemic $t_{1/2}$ for the polymerized form of TEMPO. Notably, in the hydrogel study, TEMPO was detected in the hind paw for up to 70 h, significantly longer than our result, which is to be expected due to the physical depot formed by the hydrogel. Others have investigated TEMPO conjugation to poly(ethylene glycol) (PEG),[76] hemoglobin,[77] and $\beta$-cyclodextran nanoparticles[30] to improve delivery and efficacy. TEMPO-PEG improved outcomes in a rat ischemia-reperfusion model; however, pharmacokinetics and therapeutic response was not compared to the free drug.[76] A recent study of a hemoglobin-Tempol polymer demonstrated the ability to protect endothelial cells from $O_2^{\bullet -}$-induced cell death, indicating that this system could be promising *in vivo*.[77] Tempol conjugated to $\beta$-cyclodextran nanoparticles, in combination with a $H_2O_2$-scavenging PBAP moiety, significantly improved atherosclerosis outcomes in mice over free Tempol with i.v. injections twice per week.[30] Taken together, these results demonstrate the promise of TEMPO polymers in a variety of disease conditions. However, these preparations (besides TEMPO-PEG) require more complex synthesis and formulation techniques than using a single block, unimeric polymer; higher complexity may make translation challenging, and more sophisticated carriers, particularly nanoparticles, are more apt to incur off-target effects.[78,79] An additional benefit of our system over a TEMPO-PEG or similar conjugate is the high density of active TEMPO on the polymer backbone, which demonstrated a clear benefit over lower densities (i.e., 10%) and required a lower overall polymer mass *in vivo* (i.e., 40T vs 30T). Overall, our results demonstrate that 40T is a simple formulation of TEMPO which has been optimized for therapeutic benefit in inflammation.

## CONCLUSION

This work provides a structure–function analysis of a series of DMA-*co*-TEMPO copolymers for aqueous parenteral/local and i.v. administration to treat inflammatory diseases. The balance between hydrophilic character and ROS scavenging potential proved essential to therapeutic outcomes *in vitro* and *in vivo*. Specifically, 40% TEMPO backbone density appears to be a threshold above which increased TEMPO density reduced activity. The 40T composition demonstrated improved local retention in the air pouch model of inflammation, leading to reduced TNF$\alpha$ and ROS levels, while both the 30T and 40T compositions reduced ROS levels in inflammatory footpads with i.v. administration. In both models, the polymer formulations outperformed free Tempol. The optimized random copolymer is promising to pursue for future testing in more physiologically relevant disease models and as a component of more advanced drug delivery systems such as particulate or bulk biomaterials.

# EXPERIMENTAL PROCEDURES

## Materials.

All reagents were purchased from Sigma-Aldrich unless otherwise stated. PFPA, 4-amino-TEMPO, and $\lambda$-carrageenan were purchased from TCI America. Cy5 amine was purchased from Lumiprobe. The FRAP kit was purchased from Cell BioLabs, and the Cell TiterGlo kit was purchased from Promega. TNF$\alpha$ enzyme-linked immunosorbent assay (ELISA) kit was purchased from PeproTech Inc.

## Polymer Synthesis.

Polymers were synthesized by RAFT polymerization. DMA monomer was filtered through basic alumina columns to remove radical inhibitor and stored at −20 °C for up to one month before use. DMA, PFPA, 4-cyano-4-(ethylsulfanylthiocarbonyl) sulfanylpentanoic acid (ECT, chain transfer agent (CTA)), 2,2′-azobis(isobutyronitrile) (AIBN, initiator), and trioxane (inert NMR standard) were dissolved in anhydrous dioxane. Each component was added to a flame-dried round-bottom flask under constant nitrogen stream at a final concentration of 20% (w/w) reactants. The molar ratio of monomer:CTA:initiator was 100:1:0.5. The reaction mixture was purged with nitrogen for 30 min and allowed to react for 18–24 h at 65 °C. The following day, the reaction was cooled to room temperature. 4-Amino-TEMPO (1.5 molar excess relative to PFPA units) and dipyridyldisulfide (DPDS) (1.5 molar excess relative to polymer units, added to cap the reduced trithiocarbonate CTA expected to occur upon exposure to primary amine of amino-TEMPO) were dissolved in anhydrous dimethylformamide (DMF) and added to the reaction under constant nitrogen stream. The resulting mixture was allowed to react overnight at room temperature protected from light. Polymers were purified by dialysis in methanol for 2 days (sink changed 3×/day) followed by 2 days in water (sink changed 3×/day). The resulting product was lyophilized and stored at 4 °C protected from light. Fluorescently labeled polymers were prepared as above with the inclusion of Cy5 amine (0.5 mol equiv relative to polymer units) in DMF at the TEMPO addition step.

## Polymer Characterization.

**$^{1}$H and $^{19}$F NMR.—**Samples were analyzed by NMR (Bruker) at ~1% (w/v) in deuterated chloroform ($CDCl_3$). Conversion of the DMA and PFPA monomers was confirmed by integrating the $^{1}$H NMR (400 MHz) peaks associated with acrylic protons ($\delta$ = 5.7 and 6.18 ppm for DMA and PFPA, respectively) for $t$ = 0 and $t$ = 24 h. Disappearance of these peaks was quantified relative to trioxane ($\delta$ = 5.1 ppm). $^{19}$F NMR (376 MHz) was performed on the unreacted monomer mixture, the crude RAFT product, and the purified TEMPO-functionalized polymer to confirm the presence of the PFP group on the parent polymers and the loss of the leaving group upon TEMPO conjugation.

**GPC.—**Polymer polydispersity and MW were characterized using GPC (Agilent Technologies). Polymers were dissolved at 10 mg/mL in DMF + 0.1 M LiBr mobile phase and run through three serial Tosoh Biosciences TSKGel Alpha columns at 60 °C. A Wyatt miniDAWN TREOS light scattering (Wyatt Technology Co.) and Agilent refractive index

detector were used to calculate absolute number and weight-average MW based on d$n$/d$c$ values determined on an offline refractometer (Anton Paar).

**ESR.—**ESR was used to quantify the presence of active TEMPO on each polymer backbone. Polymers were dissolved at 2 mg/mL in dimethyl sulfoxide (DMSO), and 50 μL of each sample was loaded into a glass microcapillary tube. ESR measurements were performed at room temperature using a Bruker EMXplus spectrometer (Bruker Biospin Corp. Billerica, MA). Spectrometer settings were as follows: field sweep, 120 G; center field, 3508 G; microwave frequency, 9.85 GHz; microwave power, 20 mW; modulation amplitude, 1 G; time constant 655 ms; sweep time, 121 s; receiver gain, 40 db. To quantify the nitroxide concentration, ESR spectra of the copolymers were double integrated to determine the intensity of the radical signal. Total TEMPO residue content was calculated from a standard curve of TEMPO in DMSO.

**HPLC.—**Reverse-phase HPLC (Waters) was used to determine the relative polarity of the polymers. Polymers were dissolved in a 50:50 water:acetonitrile mixture at 1 mg/mL, and 100 μL was injected utilizing a 200 μL sample loop. Samples were run through a Phenomenex C18 column (250 × 10 mm, 5 μm particle size) using a 10 min gradient from 95:5 to 0:100 water:acetonitrile, followed by 3 min at 0:100 water:acetonitrile. The retention time was recorded for each polymer using the peak UV absorbance at 310 nm.

**Octanol/Water Partition Coefficient.—**To determine the partition coefficient, 10 mg of copolymer was added to a round-bottom flask containing 5 mL each of octanol and water. The emulsion was stirred vigorously overnight and then added to a separatory funnel to collect the organic and aqueous phases. An aliquot from each phase was run on HPLC as described above, and peaks were integrated and compared to a standard to quantify the concentration of polymer in each phase. The logP value was calculated as the logarithm of the ratio of organic to aqueous phase polymer concentration.

## Cell-Free Antioxidant Activity.

**General Reducing Power.—**A commercial FRAP kit was used to determine the general antioxidant capabilities of the polymers according to the manufacturer's protocol. First, polymers were dissolved or resuspended in deionized water, and 100 μL of each sample was dispensed into a black-walled 96-well plate in triplicate. The FRAP agent was prepared by combining a 1:5 dilution of buffer, 1:10 dilution of the colorimetric probe, and a 1:10 dilution of the oxidized iron substrate with the appropriate volume of DI water. 100 μL of FRAP agent was added to each well, and the samples were incubated at room temperature for 1 h. Absorbance at 590 nm was measured on a Tecan plate reader, and background absorbance from each polymer (with no FRAP reagent added) was subtracted from the respective experimental wells. The assay was run in both a polymer mass-matched and TEMPO dose-matched format. For the former, all polymers were dissolved or resuspended at 0.4 mg/mL in DI water and plated. For the latter, all polymers and a Tempol control were dissolved or resuspended at 339 μM TEMPO in DI water and plated. Experiments were completed in triplicate.

**$O_2^{\bullet-}$ Scavenging.—**$O_2^{\bullet-}$ was generated enzymatically using the HX/XO system and detected colorimetrically using partially acetylated cytochrome C.[12] The following components were combined in the wells of a black-walled 96-well plate: 10 μL XO (0.2 U/ml), 10 μL CAT (50 μg/mL), 50 μL cytochrome C (2.4 mg/mL), and 10 μL polymers. Polymers were used at the same mass-matched and dose-matched concentrations as for the FRAP assay. SOD (final concentration 200 U/mL) and 1× phosphate buffered saline (PBS) were used as negative and positive controls, respectively. CAT was included to scavenge $H_2O_2$ generated in the reaction.[39] HX was dissolved at 6.80 mg/mL in 1 M sodium hydroxide (NaOH) and diluted 1:100 in PBS. To initiate the enzymatic reaction, 20 μL HX was added to each well, and absorbance was measured immediately and every 10 min thereafter for 60 min on a Tecan plate reader at 550 nm. Background absorbance from the polymers was measured from non-$O_2^{\bullet-}$ containing wells and subtracted from the experimental data for each respective polymer.

### *In Vitro* Activity.

**Cell Culture.—**ATDC5 chondrogenic cells were maintained in Dulbecco's Modified Eagles Medium (DMEM)/F12 supplemented with 10% fetal bovine serum (FBS) and 1% penicillin/streptomycin (P/S) at 37 °C, 5% $CO_2$. Subconfluent (80%) cultures were passaged using 0.25% trypsin to detach cells at a seeding ratio of 1:10.

**Cytocompatibility.—**ATDC5 chondrocyte-like cells were seeded at 10,000 cells/well in black-walled 96-well plates in dye-free DMEM + 1% FBS and 1% P/S. After adhering overnight, the cells were washed with 1× PBS and treated with 100 μL polymers at 0.1, 1, and 5 mg/mL. After 24 h, treatments were removed, and viability was assessed using a commercial CellTiter-Glo kit (Promega) according to the manufacturer's directions. Briefly, the substrate was reconstituted in assay buffer, and 100 μL was added to each well. After a 10 min incubation at room temperature, luminescence was imaged on an *In Vivo* Imaging System (IVIS). Signal was normalized to media-treated cells.

**Polymer Cell Uptake Visualization by Confocal Microscopy.—**ATDC5 cells (20,000) were seeded onto an 8-well chambered coverglass (#1 German borosilicate, Nunc LabTek) and allowed to adhere overnight. Cells were washed with PBS and then treated for 24 h with 250 μg/mL Cy5-labeled polymers dissolved in DMEM + 1% FBS + 1% P/S. After incubation, cells were washed with PBS, fixed with 4% paraformaldehyde in PBS (Alfa Aesar) for 25 min, washed again with PBS, stained with DAPI (NucBlue Fixed Cell Stain ReadyProbes, Invitrogen) based upon manufacturer directions, washed again with PBS, and overlaid with 25 mM tris(2-carboxyethyl)phosphine-supplemented PBS to reduce extracellular fluorescence of Cy5 as previously described.[80] Finally, cells were imaged with a confocal scanning laser microscope (Nikon Eclipse Ti Microscope with D-Eclipse C1 laser, Nikon Instruments, Inc.) using a 405 nm (blue) and 640 nm (red) laser line. Resulting images were processed by splitting the blue and red channels and merging images.

**Polymer Cell Uptake Quantification by ESR.—**ATDC5 cells were seeded at $1 \times 10^6$ cells/flask in T75 flasks and allowed to adhere overnight. Polymers or Tempol were dissolved at 0.4 mg/mL in phenol red-free, supplement-free DMEM, and 10 mL treatments

were applied to the flasks. After 24 h, cells were lifted by scraping and collected in 15 mL centrifuge tubes. Cells were pelleted at 500×*g* for 5 min, and supernatant was removed by aspiration. To lyse cells and release polymers, pellets were suspended in 200 μL DMSO. Samples were frozen at −80 °C until analysis. For analysis of uptake, samples were thawed, vortexed, and scanned by ESR as described above. Signals were normalized to inherent ESR signal of each polymer to quantify uptake. Polymers with TEMPO content >40% could not be evaluated for cell uptake, because they were insoluble in cell culture media, precipitating to form insoluble aggregates that could not be separated from cells prior to measurement.

**Protection from ROS-Induced Cell Death.—**ATDC5 were seeded at 10,000 cells/well and allowed to adhere overnight. Cells were co-treated with polymers and 1 mM SIN-1 in dye-free DMEM + 1% FBS and 1% P/S for 24 h. SIN-1 was used to induce ROS toxicity, as it spontaneously decomposes to $O_2^{\bullet -}$ and $NO^{\bullet}$ in aqueous media.[48] Polymer treatments were matched to polymer mass at 0.2 mg/mL or TEMPO dose at 170 μM as described above. Cell viability was measured using the CellTiter-Glo kit on the IVIS as described above and normalized to cells treated with media containing neither SIN-1 nor polymers.

### *In Vivo* Anti-Inflammatory Activity.

**Inflammatory Air Pouch Procedure.—**All protocols were approved by the Institutional Animal Care and Use Committee of Vanderbilt University and done in accordance with the National Institutes of Health Guide for the Care and Use of Laboratory Animals. The anti-inflammatory effect of the polymers was tested in the murine air pouch model of inflammation[60] with slight modifications. Ten-week-old C57Bl/6 mice were obtained and allowed to acclimate for 3 days. Animals were kept on a 12 h light/dark cycle and allowed free access to food and water. All experiments were performed under isoflurane anesthesia. On day 0 of the experiment, mice received a subcutaneous injection of 5 mL sterile air on the dorsal region. On day 3, mice were reinjected with 3 mL sterile air. On day 5, 0.5% λ-carrageenan was prepared by dissolving 500 mg carrageenan in 100 mL 0.9% sterile saline with vigorous stirring and heating to 90 °C. The solution was sterilized by autoclaving. On day 6 of the experiment, mice received a 1 mL injection into the pouch of carrageenan ± treatments (5–6 mice per group). Five treatment groups were compared: saline, 0.5% carrageenan, 0.5% carrageenan + 40T, 0.5% carrageenan + 100T, and 0.5% carrageenan + Tempol. All TEMPO treatments were dissolved in carrageenan at 8.48 mM TEMPO (40T, 100T, and Tempol at 5.0, 2.7, and 1.46 mg/mL, respectively). Treatments were prepared immediately prior to injection.

**Retention and Anti-Inflammatory Effects after Air Pouch Inflammation.—**Mice were sacrificed at 6 or 24 h after carrageenan ± treatment injection by $CO_2$ inhalation. The pouch was rinsed with 1 mL sterile 5.4 mM ethylenediaminetetraacetic acid (EDTA) to collect the inflammatory exudate. A 100 μL aliquot was collected and frozen at −20 °C for ESR measurement of polymer retention. Cells were pelleted with centrifugation at 500×*g* for 5 min, and a 100 μL aliquot of the supernatant was frozen at −80 °C for ELISA. Fresh supernatant was plated at 50 μL/well in a black-walled 96-well plate. Cytochrome C (50 μL, 2.4 mg/mL) was added, and absorbance at 550 nm was measured every 10 min for 60 min. For ELISAs, TNFα was measured in the supernatant using a commercial sandwich ELISA

kit (PeproTech) according to the manufacturer's directions. Briefly, capture antibody was applied to the plate, followed by sample, biotinylated detection antibody, avidin-horseradish peroxidase (HRP), and finally 2,2′-azinobis[3-ethylbenzothiazoline-6-sulfonic acid]-diammonium salt liquid substrate. Absorbance at 405 nm with correction at 650 nm was measured every 5 min for 45 min.

**Intravital Microscopy and Biodistribution with Intravenous Delivery.—**Intravital microscopy (IVM) was used to measure the distribution $t_{1/2}$ of the hydrophilic copolymers (40T, 30T, 20T, and 10T) as described previously.[81] Briefly, male C57Bl/6 mice ($n = 3$ per group) were anesthetized with isoflurane and placed on the heated stage of a confocal microscope (Nikon). The ear was cleaned, and the microscope was focused on the veins in the ear. The mouse was injected with 100 μL Cy5-labeled copolymer solution in saline (10 mg/kg), and Cy5 fluorescence was monitored continuously. To measure $t_{1/2}$, a circular region of interest was highlighted within the vessel and signal intensity was measured over time within the region. The PKSolver plugin within Microsoft Excel software was used to calculate $t_{1/2}$ using a nonlinear regression one-compartment model.[82] To investigate biodistribution, polymers were injected i.v. at 10 mg/kg, and animals were sacrificed after 10 min. Heart, lungs, kidneys, liver, and spleen were removed to a Petri dish and imaged for Cy5 fluorescence by IVIS. Signal was measured by drawing a region of interest around each organ and measuring the total radiant efficiency. The signal for each organ was normalized to the total signal from all organs.

**Footpad Inflammation Model.—**Female and male C57BL/6 mice were used for development of footpad inflammation to study systemic administration of DMA-*co*-TEMPO copolymers. A 1% λ-carrageenan solution was prepared by mixing 10 mg λ-carrageenan powder with 1 mL 0.9% saline in a sterile vial. After gentle swirling, the vial was left uninterrupted for 16 h at room temperature. The resultant carrageenan solution (50 μL) was injected into the rear right footpad under isoflurane anesthesia. Control animals received no injection. After 6 h to establish inflammation, animals received an i.v. injection of saline or treatment. Five treatment groups were compared ($n = 5–7$ mice per group): no injection, carrageenan + saline, carrageenan + Tempol, carrageenan + 40T, and carrageenan + 30T. All TEMPO treatments were dissolved at 3.77 mM TEMPO (0.65, 2.0, and 2.63 mg/mL for Tempol, 40T, and 30T, respectively), and the injection volume was 100 μL.

**In Vivo Measurement of ROS.—**Luminol sodium salt was used to measure ROS levels in the inflamed footpad.[83] The probe was dissolved at 50 mg/mL in sterile saline and protected from light throughout the experiment. Fifteen minutes after i.v. treatment administration, 100 μL of luminol was injected subcutaneously in the dorsal region. Signal was allowed to develop for 15 min, and bioluminescence was imaged by IVIS.

## Statistical Analysis.

All data are reported as mean ± standard deviation. Student's *t* test was used to determine statistical significance between two groups. Analysis of variance (ANOVA) with a Tukey posthoc test for multiple comparisons was used to compare three or more groups. $p < 0.05$ was considered significant. For the inflammatory footpad procedure, a Grubb's test was

performed to identify statistical outliers, and one outlier was removed from the 30T group for the luminol measurement. All statistical analysis was performed in GraphPad Prism.

## Supplementary Material

Refer to Web version on PubMed Central for supplementary material.

## ACKNOWLEDGMENTS

We gratefully acknowledge the Vanderbilt Free Radicals in Medicine Core (FRIMCORE) for ESR measurements, the Vanderbilt Small Molecule NMR Facility Core for NMR scans, and the Vanderbilt University Institute of Imaging Science (VUIIS) for use of the IVIS equipment. This work was supported by the National Science Foundation (NSF) award nos. DGE-1937963, DMR-1852157, and DMR BMAT 1349604. Additional support was provided by the National Institutes of Health (NIH) National Institute of Biomedical Imaging and Bioengineering (NIBIB) training grant no. T32-EB021937, NIH RO1 EB028690, and NIH P01HL129941.

## ABBREVIATIONS

| | |
|---|---|
| **AIBN, 2** | 2′-azobis(isobutyronitrile) |
| **ANOVA** | analysis of variance |
| **CAT** | catalase |
| **$CDCl_3$** | deuterated chloroform |
| **COX2** | cyclooxygenase-2 |
| **CTA** | chain transfer agent |
| **Cy5** | cyanine5 |
| **DMA, *N*** | *N*-dimethylacrylamide |
| **DMEM** | Dulbecco’s Modified Eagles Medium |
| **DMF** | dimethylformamide |
| **DMFO** | 4*b*,9*b*-dihydroxy-6-methoxy-8-(3-oxo-but-1-enyl)-4*b*,9*b*-dihydro-5-oxa-indeno[2,1-*a*]inden-10-one |
| **DMSO** | dimethyl sulfoxide |
| **DPDS** | dipyridyldisulfide |
| **ECT** | 4-cyano-4-(ethylsulfanylthiocaronyl) sulfanylpentanoic acid |
| **EDTA** | ethylenediaminetetraacetic acid |
| **ELISA** | enzyme-linked immunosorbent assay |
| **ELVIS** | extravasation through leaky vasculature and the subsequent inflammatory cell-mediated sequestration |
| **EPR** | enhanced permeation and retention |

| | |
|---|---|
| **ESR** | electron spin resonance |
| **FBS** | fetal bovine serum |
| **FRAP** | ferric reducing antioxidant power |
| **GPX** | glutathione peroxidase |
| **$H_2O_2$** | hydrogen peroxide |
| **HX** | hypoxanthine |
| **i.v.** | intravenous |
| **IVIS** | *in vivo* imaging system |
| **IVM** | intravital microscopy |
| **logP** | octanol–water partition coefficient |
| **LPS** | lipopolysaccharide |
| **MAPK** | p38 mitogen-activated protein kinase |
| **MSC** | mesenchymal stem cells |
| **MW** | molecular weight |
| **NF-κB** | nuclear factor κ-light-chain-enhancer of activated B cells |
| **$NO^{\bullet}$** | nitric oxide |
| **Nrf2** | nuclear factor erythroid 2-related factor 2 |
| **$OCl^{-}$** | hypochlorite ion |
| **$OH^{\bullet}$** | hydroxyl radical |
| **$O_2^{\bullet-}$** | superoxide |
| **P/S** | penicillin/streptomycin |
| **PBAP** | phenylboronic acid pinacol ester |
| **PBS** | phosphate buffered saline |
| **PCMS** | poly(chloromethylstyrene) |
| **PEG** | poly(ethylene glycol) |
| **PFP** | pentafluorophenyl |
| **PFPA** | pentafluorophenyl acrylate |
| **Plvap** | plasmalemmal vesicle-associated protein |
| **POx** | poly(2-oxazoline) |

| | |
|---|---|
| **PPS** | poly(propylene sulfide) |
| **RA** | rheumatoid arthritis |
| **RAFT** | reversible addition–fragmentation chain transfer |
| **ROS** | reactive oxygen species |
| **SIN-1** | 3-morpholinosidnonimine |
| **SkQ1** | 10-(6′-plastoquinonyl)decyltriphenylphosphonium |
| **SOD** | superoxide dismutase |
| $T_{1/2}$ | half-life |
| **TBHP** | *tert*-butyl hydroperoxide |
| **TEMPO** | 2,2,6,6-tetramethylpiperidine-1-oxyl |
| **TNF$\alpha$** | tumor necrosis factor $\alpha$ |
| **VIP** | vasoactive intestinal peptide |
| **XO** | xanthine oxidase |

## REFERENCES


(1). Halliwell B. (1991) Reactive oxygen species in living systems: Source, biochemistry, and role in human disease. Am. J. Med 91 (3), S14–S22.

(2). D'Autréaux B, and Toledano MB (2007) ROS as signalling molecules: mechanisms that generate specificity in ROS homeostasis. Nat. Rev. Mol. Cell Biol 8 (10), 813–824. [PubMed: 17848967]

(3). Chapple ILC (1997) Reactive oxygen species and antioxidants in inflammatory diseases. J. Clin. Periodontol 24 (5), 287–296. [PubMed: 9178107]

(4). El-Mohtadi F, d'Arcy R, and Tirelli N. (2019) Oxidation-Responsive Materials: Biological Rationale, State of the Art, Multiple Responsiveness, and Open Issues. Macromol. Rapid Commun 40 (1), 1800699.

(5). Bauerova K, and Bezek S. (2000) Role of reactive oxygen and nitrogen species in etiopathogenesis of rheumatoid arthritis. Gen. Physiol. Biophys 18, 15–20.

(6). Pelicano H, Carney D, and Huang P. (2004) ROS stress in cancer cells and therapeutic implications. Drug Resist. Updates 7 (2), 97–110.

(7). Newsholme P, Cruzat VF, Keane KN, Carlessi R, and de Bittencourt PIH Jr. (2016) Molecular mechanisms of ROS production and oxidative stress in diabetes. Biochem. J 473 (24), 4527–4550. [PubMed: 27941030]

(8). Bonomini F, Tengattini S, Fabiano A, Bianchi R, and Rezzani R. (2008) Atherosclerosis and oxidative stress. Histol. Histopathol 23, 3.

(9). Blaser H, Dostert C, Mak TW, and Brenner D. (2016) TNF and ROS Crosstalk in Inflammation. Trends Cell Biol. 26 (4), 249–261. [PubMed: 26791157]

(10). Simon HU, Haj-Yehia A, and Levi-Schaffer F. (2000) Role of reactive oxygen species (ROS) in apoptosis induction. Apoptosis 5 (5), 415–418. [PubMed: 11256882]

(11). Birben E, Sahiner UM, Sackesen C, Erzurum S, and Kalayci O. (2012) Oxidative Stress and Antioxidant Defense. World Allergy Organ. J 5 (1), 9–19. [PubMed: 23268465]

(12). McCord JM, and Fridovich I. (1969) Superoxide Dismutase: An Enzymatic Function for Erythrocuprein (Hemocuprein). J. Biol. Chem 244 (22), 6049–6055. [PubMed: 5389100]

(13). Liu TH, Beckman JS, Freeman BA, Hogan EL, and Hsu CY (1989) Polyethylene glycol-conjugated superoxide dismutase and catalase reduce ischemic brain injury. Am. J. Physiol 256 (2), H589–H593. [PubMed: 2492771]

(14). Seshadri G, Sy JC, Brown M, Dikalov S, Yang SC, Murthy N, and Davis ME (2010) The delivery of superoxide dismutase encapsulated in polyketal microparticles to rat myocardium and protection from myocardial ischemia-reperfusion injury. Biomaterials 31 (6), 1372–1379. [PubMed: 19889454]

(15). Laukkanen MO, Leppanen P, Turunen P, Tuomisto T, Naarala J, and Yla-Herttuala S. (2001) EC-SOD gene therapy reduces paracetamol-induced liver damage in mice. J. Gene Med 3 (4), 321–325. [PubMed: 11529661]

(16). Tanaka M, Kogawa K, Nakamura K, Nishihori Y, Kuribayashi K, Hagiwara S, Muramatsu H, Sakamaki S, and Niitsu Y. (2001) Anti-metastatic gene therapy utilizing subcutaneous inoculation of EC-SOD gene transduced autologous fibroblast suppressed lung metastasis of Meth-A cells and 3LL cells in mice. Gene Ther. 8 (2), 149–156. [PubMed: 11313784]

(17). Beckman JS, Minor RL Jr., White CW, Repine JE, Rosen GM, and Freeman BA (1988) Superoxide Dismutase and Catalase Conjugated to Polyethylene Glycol Increases Endothelial Enzyme Activity and Oxidant Resistance. J. Biol. Chem 263 (14), 6884–6892. [PubMed: 3129432]

(18). Shuvaev VV, Han J, Yu KJ, Huang S, Hawkins BJ, Madesh M, Nakada M, and Muzykantov VR (2011) PECAM-targeted delivery of SOD inhibits endothelial inflammatory response. FASEB J. 25 (1), 348–357. [PubMed: 20876216]

(19). Shuvaev VV, Kiseleva RY, Arguiri E, Villa CH, Muro S, Christofidou-Solomidou M, Stan RV, and Muzykantov VR (2018) Targeting superoxide dismutase to endothelial caveolae profoundly alleviates inflammation caused by endotoxin. J. Controlled Release 272, 1–8.

(20). Kost OA, Beznos OV, Davydova NG, Manickam DS, Nikolskaya II, Guller AE, Binevski PV, Chesnokova NB, Shekhter AB, Klyachko NL, and Kabanov AV (2016) Superoxide Dismutase 1 Nanozyme for Treatment of Eye Inflammation. Oxid. Med. Cell. Longevity 2016, 1.

(21). Tong J, Yi X, Luxenhofer R, Banks WA, Jordan R, Zimmerman MC, and Kabanov AV (2013) Conjugates of Superoxide Dismutase 1 with Amphiphilic Poly(2-oxazoline) Block Copolymers for Enhanced Brain Delivery: Synthesis, Characterization and Evaluation in Vitro and in Vivo. Mol. Pharmaceutics 10 (1), 360–377.

(22). Oda T, Akaike T, Hamamoto T, Suzuki F, Hirano T, and Maeda H. (1989) Oxygen radicals in influenza-induced pathogenesis and treatment with pyran polymer-conjugated SOD. Science 244 (4907), 974. [PubMed: 2543070]

(23). Trnka J, Blaikie FH, Smith RAJ, and Murphy MP (2008) A mitochondria-targeted nitroxide is reduced to its hydroxylamine by ubiquinol in mitochondria. Free Radical Biol. Med 44 (7), 1406–1419. [PubMed: 18206669]

(24). Ni R, Cao T, Xiong S, Ma J, Fan G-C, Lacefield JC, Lu Y, Tissier SL, and Peng T. (2016) Therapeutic inhibition of mitochondrial reactive oxygen species with mito-TEMPO reduces diabetic cardiomyopathy. Free Radical Biol. Med 90, 12–23. [PubMed: 26577173]

(25). Dikalova AE, Bikineyeva AT, Budzyn K, Nazarewicz RR, McCann L, Lewis W, Harrison DG, and Dikalov SI (2010) Therapeutic targeting of mitochondrial superoxide in hypertension. Circ. Res 107 (1), 106–116. [PubMed: 20448215]

(26). Du K, Farhood A, and Jaeschke H. (2017) Mitochondria-targeted antioxidant Mito-Tempo protects against acetaminophen hepatotoxicity. Arch. Toxicol 91 (2), 761–773. [PubMed: 27002509]

(27). Zhang J, Wang Q, Xu C, Lu Y, Hu H, Qin B, Wang Y, He D, Li C, Yu X, Wang S, and Liu J. (2017) MitoTEMPO Prevents Oxalate Induced Injury in NRK-52E Cells via Inhibiting Mitochondrial Dysfunction and Modulating Oxidative Stress. Oxid. Med. Cell. Longevity 2017, 1.

(28). Liu Y, Wang Y, Ding W, and Wang Y. (2018) Mito-TEMPO Alleviates Renal Fibrosis by Reducing Inflammation, Mitochondrial Dysfunction, and Endoplasmic Reticulum Stress. Oxid. Med. Cell. Longevity 2018, 1.

(29). Yoshitomi T, and Nagasaki Y. (2011) Nitroxyl radical-containing nanoparticles for novel nanomedicine against oxidative stress injury. Nanomedicine 6 (3), 509–518. [PubMed: 21542688]

(30). Wang Y, Li L, Zhao W, Dou Y, An H, Tao H, Xu X, Jia Y, Lu S, Zhang J, and Hu H. (2018) Targeted Therapy of Atherosclerosis by a Broad-Spectrum Reactive Oxygen Species Scavenging Nanoparticle with Intrinsic Anti-inflammatory Activity. ACS Nano 12 (9), 8943–8960. [PubMed: 30114351]

(31). Pua ML, Yoshitomi T, Chonpathompikunlert P, Hirayama A, and Nagasaki Y. (2013) Redox-active injectable gel using thermoresponsive nanoscale polyion complex flower micelle for noninvasive treatment of local inflammation. J. Controlled Release 172 (3), 914–920.

(32). Eberhardt M, Mruk R, Zentel R, and Théato P. (2005) Synthesis of pentafluorophenyl(meth)acrylate polymers: New precursor polymers for the synthesis of multifunctional materials. Eur. Polym. J 41 (7), 1569–1575.

(33). Yoshitomi T, Kuramochi K, Binh Vong L, and Nagasaki Y. (2014) Development of nitroxide radicals-containing polymer for scavenging reactive oxygen species from cigarette smoke. Sci. Technol. Adv. Mater 15 (3), 035002–035002.

(34). Yoshitomi T, Miyamoto D, and Nagasaki Y. (2009) Design of Core–Shell-Type Nanoparticles Carrying Stable Radicals in the Core. Biomacromolecules 10 (3), 596–601. [PubMed: 19191564]

(35). Voest EE, Faassen E. v., and Marx JJM (1993) An electron paramagnetic resonance study of the antioxidant properties of the nitroxide free radical tempo. Free Radical Biol. Med 15 (6), 589–595. [PubMed: 8138184]

(36). Berliner LJ, Khramtsov V, Fujii H, and Clanton TL (2001) Unique in vivo applications of spin traps. Free Radical Biol. Med 30 (5), 489–499. [PubMed: 11182519]

(37). Yoshida E, and Tanaka T. (2006) Oxidation-induced micellization of a diblock copolymer containing stable nitroxyl radicals. Colloid Polym. Sci 285 (2), 135–144.

(38). Benzie IFF, and Strain JJ (1996) The Ferric Reducing Ability of Plasma (FRAP) as a Measure of "Antioxidant Power": The FRAP Assay. Anal. Biochem 239 (1), 70–76. [PubMed: 8660627]

(39). Fridovich I. (1970) Quantitative Aspects of the Production of Superoxide Anion Radical by Milk Xanthine Oxidase. J. Biol. Chem 245 (16), 4053–4057. [PubMed: 5496991]

(40). Yoshitomi T, Yamaguchi Y, Kikuchi A, and Nagasaki Y. (2012) Creation of a blood-compatible surface: A novel strategy for suppressing blood activation and coagulation using a nitroxide radical-containing polymer with reactive oxygen species scavenging activity. Acta Biomater. 8 (3), 1323–1329. [PubMed: 22155332]

(41). Dikalov SI, Dikalova AE, Morozov DA, and Kirilyuk IA (2018) Cellular accumulation and antioxidant activity of acetoxymethoxycarbonyl pyrrolidine nitroxides. Free Radical Res. 52 (3), 339–350. [PubMed: 29098905]

(42). Luxenhofer R, Sahay G, Schulz A, Alakhova D, Bronich TK, Jordan R, and Kabanov AV (2011) Structure-property relationship in cytotoxicity and cell uptake of poly(2-oxazoline) amphiphiles. J. Controlled Release 153 (1), 73–82.

(43). Batrakova EV, Li S, Alakhov VY, Miller DW, and Kabanov AV (2003) Optimal Structure Requirements for Pluronic Block Copolymers in Modifying P-glycoprotein Drug Efflux Transporter Activity in Bovine Brain Microvessel Endothelial Cells. J. Pharmacol. Exp. Ther 304 (2), 845. [PubMed: 12538842]

(44). Dailing EA, Kilchrist KV, Tierney JW, Fletcher RB, Evans BC, and Duvall CL (2020) Modifying Cell Membranes with Anionic Polymer Amphiphiles Potentiates Intracellular Delivery of Cationic Peptides. ACS Appl. Mater. Interfaces 12 (45), 50222–50235.

(45). Swartz HM, Sentjurc M, and Morse PD (1986) Cellular metabolism of water-soluble nitroxides: Effect on rate of reduction of cell/nitroxide ratio, oxygen concentrations and permeability of nitroxides. Biochim. Biophys. Acta, Mol. Cell Res 888 (1), 82–90.

(46). Thirunavukkarasu C, Watkins S, Harvey SAK, and Gandhi CR (2004) Superoxide-induced apoptosis of activated rat hepatic stellate cells. J. Hepatol 41 (4), 567–575. [PubMed: 15464236]

(47). Jameel NM, Thirunavukkarasu C, Wu T, Watkins SC, Friedman SL, and Gandhi CR (2009) p38-MAPK- and caspase-3-mediated superoxide-induced apoptosis of rat hepatic stellate cells: Reversal by retinoic acid. J. Cell. Physiol 218 (1), 157–166. [PubMed: 18792915]

(48). Gergel D, Misik V, Ondrias K, and Cederbaum AI (1995) Increased Cytotoxicity of 3-Morpholinosydnonimine to HepG2 Cells in the Presence of Superoxide Dismutase. J. Biol. Chem 270 (36), 20922–20929. [PubMed: 7673115]

(49). Martin-Romero FJ, Gutiérrez-Martin Y, Henao F, and Gutiérrez-Merino C. (2004) Fluorescence measurements of steady state peroxynitrite production upon SIN-1 decomposition: NADH versus dihydrodichlorofluorescein and dihydrorhodamine 123. J. Fluoresc 14 (1), 17–23. [PubMed: 15622856]

(50). Carroll RT, Galatsis P, Borosky S, Kopec KK, Kumar V, Althaus JS, and Hall ED (2000) 4-Hydroxy-2,2,6,6-tetramethylpiperidine-1-oxyl (Tempol) Inhibits Peroxynitrite-Mediated Phenol Nitration. Chem. Res. Toxicol 13 (4), 294–300. [PubMed: 10775330]

(51). Napoli A, Valentini M, Tirelli N, Müller M, and Hubbell JA (2004) Oxidation-responsive polymeric vesicles. Nat. Mater 3 (3), 183–189. [PubMed: 14991021]

(52). Gupta MK, Martin JR, Werfel TA, Shen T, Page JM, and Duvall CL (2014) Cell Protective, ABC Triblock Polymer-Based Thermoresponsive Hydrogels with ROS-Triggered Degradation and Drug Release. J. Am. Chem. Soc 136 (42), 14896–14902. [PubMed: 25254509]

(53). Poole KM, Nelson CE, Joshi RV, Martin JR, Gupta MK, Haws SC, Kavanaugh TE, Skala MC, and Duvall CL (2015) ROS-responsive microspheres for on demand antioxidant therapy in a model of diabetic peripheral arterial disease. Biomaterials 41, 166–175. [PubMed: 25522975]

(54). Dollinger BR, Gupta MK, Martin JR, and Duvall CL (2017) Reactive Oxygen Species Shielding Hydrogel for the Delivery of Adherent and Nonadherent Therapeutic Cell Types. Tissue Eng., Part A 23 (19−20), 1120–1131.

(55). SLAMEOVA D (2003) Protective effects of fungal (1→3)-β-d-glucan derivatives against oxidative DNA lesions in V79 hamster lung cells. Cancer Lett. 198 (2), 153–160. [PubMed: 12957353]

(56). Wong VW, Rustad KC, Glotzbach JP, Sorkin M, Inayathullah M, Major MR, Longaker MT, Rajadas J, and Gurtner GC (2011) Pullulan Hydrogels Improve Mesenchymal Stem Cell Delivery into High-Oxidative-Stress Wounds. Macromol. Biosci 11 (11), 1458–1466. [PubMed: 21994074]

(57). Kim Y, Choi Y, Ham H, Jeong H-S, and Lee J. (2013) Protective effects of oligomeric and polymeric procyanidin fractions from defatted grape seeds on tert-butyl hydroperoxide-induced oxidative damage in HepG2 cells. Food Chem. 137 (1), 136–141. [PubMed: 23200001]

(58). Chen H-M, and Yan X-J (2005) Antioxidant activities of agaro-oligosaccharides with different degrees of polymerization in cell-based system. Biochim. Biophys. Acta, Gen. Subj 1722 (1), 103–111.

(59). Rajkovic O, Gourmel C, d'Arcy R, Wong R, Rajkovic I, Tirelli N, and Pinteaux E. (2019) Reactive Oxygen Species-Responsive Nanoparticles for the Treatment of Ischemic Stroke. Adv. Ther 2 (7), 1900038.

(60). Duarte DB, Vasko MR, and Fehrenbacher JC (2012) Models of Inflammation: Carrageenan Air Pouch. Curr. Protoc. Pharmacol 56 (1), 5.6.1–5.6.8.

(61). Chelombitko MA, Averina OA, Vasil'eva TV, Dvorianinova EE, Egorov MV, Pletjushkina OY, Popova EN, Fedorov AV, Romashchenko VP, and Ilyinskaya OP (2017) Comparison of the Effects of Mitochondria-Targeted Antioxidant 10-(6′-Plastoquinonyl)Decyltriphenylphosphonium Bromide (SkQ1) and a Fragment of its Molecule Dodecyltriphenylphosphonium on Carrageenan-Induced Acute Inflammation in Mouse Model of Subcuteneous Air Pouch. Bull. Exp. Biol. Med 162 (6), 730–733. [PubMed: 28429222]

(62). Sunita P, Jha S, and Pattanayak SP (2011) Anti-inflammatory and in-vivo Antioxidant activities of Cressa cretica Linn., a halophytic plant. Middle East J. Sci. Res 8 (1), 129–140.

(63). Menshchikova EB, Zenkov NK, Tkachev VO, Lemza AE, and Kandalintseva NV (2013) Protective Effect of ARE-Inducing Phenol Antioxidant TS-13 in Chronic Inflammation. Bull. Exp. Biol. Med 155 (3), 330–334. [PubMed: 24137596]

(64). El-Achkar GA, Mrad MF, Mouawad CA, Badran B, Jaffa AA, Motterlini R, Hamade E, and Habib A. (2019) Heme oxygenase-1—Dependent anti-inflammatory effects of atorvastatin in zymosan-injected subcutaneous air pouch in mice. PLoS One 14 (5), e0216405.

(65). Mathew G, Sharma A, Pickering RJ, Rosado CJ, Lemarie J, Mudgal J, Thambi M, Sebastian S, Jandeleit-Dahm KA, de Haan JB, and Unnikrishnan MK (2018) A novel synthetic small molecule DMFO targets Nrf2 in modulating proinflammatory/antioxidant mediators to ameliorate inflammation. Free Radical Res. 52 (10), 1140–1157. [PubMed: 30422019]

(66). Komarov AM, Joseph J, and Lai C-S (1994) In vivo pharmacokinetics of nitroxides in mice. Biochem. Biophys. Res. Commun 201 (2), 1035–1042. [PubMed: 8002974]

(67). Uddin MJ, Werfel TA, Crews BC, Gupta MK, Kavanaugh TE, Kingsley PJ, Boyd K, Marnett LJ, and Duvall CL (2016) Fluorocoxib A loaded nanoparticles enable targeted visualization of cyclooxygenase-2 in inflammation and cancer. Biomaterials 92, 71–80. [PubMed: 27043768]

(68). Tan J, Deng Z, Liu G, Hu J, and Liu S. (2018) Anti-inflammatory polymersomes of redox-responsive polyprodrug amphiphiles with inflammation-triggered indomethacin release characteristics. Biomaterials 178, 608–619. [PubMed: 29605185]

(69). Koziolová E, Venclíková K, and Etrych T. (2018) Polymer-drug conjugates in inflammation treatment. Physiol. Res 67, S281. [PubMed: 30379550]

(70). Yuan F, Quan L. d., Cui L, Goldring SR, and Wang D. (2012) Development of macromolecular prodrug for rheumatoid arthritis. Adv. Drug Delivery Rev 64 (12), 1205–1219.

(71). Maeda H, Wu J, Sawa T, Matsumura Y, and Hori K. (2000) Tumor vascular permeability and the EPR effect in macromolecular therapeutics: a review. J. Controlled Release 65 (1), 271–284.

(72). Maeda H. (2012) Vascular permeability in cancer and infection as related to macromolecular drug delivery, with emphasis on the EPR effect for tumor-selective drug targeting. Proc. Jpn. Acad., Ser. B 88 (3), 53–71. [PubMed: 22450535]

(73). Chedid P, Boussetta T, Dang PMC, Belambri SA, Marzaioli V, Fasseau M, Walker F, Couvineau A, El-Benna J, and Marie JC (2017) Vasoactive intestinal peptide dampens formylpeptide-induced ROS production and inflammation by targeting a MAPK-p47phox phosphorylation pathway in monocytes. Mucosal Immunol. 10 (2), 332–340. [PubMed: 27271317]

(74). Dragojevic-Simic V, Jacevic V, Dobric S, Djordjevic A, Bokonjic D, Bajcetic M, and Injac R. (2011) Anti-Inflammatory Activity of Fullerenol C 60 (OH) 24 Nano-Particles in a Model of Acute Inflammation in Rats. Digest J. Nanomater. Biostruct 6 (2), 1.

(75). Ik A, Fleischer TC, Annan K, Dickson RA, Mensah AY, and Sarpong FM (2013) Anti-inflammatory, antioxidant and antimicrobial activity of the stem bark extract and fractions of Ficus exasperata Vahl.(Moraceae). J. Pharmacog. Phytochem 2 (3), 38–44.

(76). Bi W, Li X, Bi Y, Xue P, Zhang Y, Gao X, Wang Z, Li M, Itagaki Y, and Bi L. (2012) Novel TEMPO-PEG-RGDs Conjugates Remediate Tissue Damage Induced by Acute Limb Ischemia/Reperfusion. J. Med. Chem 55 (9), 4501–4505. [PubMed: 22439897]

(77). Wu M, Feng K, Li Q, Ma H, Zhu H, Xie Y, Yan G, Chen C, and Yan K. (2018) Glutaraldehyde-polymerized hemoglobin and tempol (PolyHb-tempol) has superoxide dismutase activity that can attenuate oxidative stress on endothelial cells induced by superoxide anion. Artif. Cells, Nanomed., Biotechnol 46 (1), 47–55. [PubMed: 28521553]

(78). Parhiz H, Khoshnejad M, Myerson JW, Hood E, Patel PN, Brenner JS, and Muzykantov VR (2018) Unintended effects of drug carriers: Big issues of small particles. Adv. Drug Delivery Rev 130, 90–112.

(79). Jackson MA, Patel SS, Yu F, Cottam MA, Glass EB, Hoogenboezem EN, Fletcher RB, Dollinger BR, Patil P, Liu DD, Kelly IB, Bedingfield SK, King AR, Miles RE, Hasty AM, Giorgio TD, and Duvall CL (2021) Kupffer cell release of platelet activating factor drives dose limiting toxicities of nucleic acid nanocarriers. Biomaterials 268, 120528.

(80). Vaughan JC, Dempsey GT, Sun E, and Zhuang X. (2013) Phosphine quenching of cyanine dyes as a versatile tool for fluorescence microscopy. J. Am. Chem. Soc 135 (4), 1197–1200. [PubMed: 23311875]

(81). Jackson MA, Werfel TA, Curvino EJ, Yu F, Kavanaugh TE, Sarett SM, Dockery MD, Kilchrist KV, Jackson AN, Giorgio TD, and Duvall CL (2017) Zwitterionic Nanocarrier Surface Chemistry Improves siRNA Tumor Delivery and Silencing Activity Relative to Polyethylene Glycol. ACS Nano 11 (6), 5680–5696. [PubMed: 28548843]

(82). Zhang Y, Huo M, Zhou J, and Xie S. (2010) PKSolver: An add-in program for pharmacokinetic and pharmacodynamic data analysis in Microsoft Excel. Comp. Methods Prog. Biomed 99 (3), 306–314.

(83). Liu WF, Ma M, Bratlie KM, Dang TT, Langer R, and Anderson DG (2011) Real-time in vivo detection of biomaterial-induced reactive oxygen species. Biomaterials 32 (7), 1796–1801. [PubMed: 21146868]

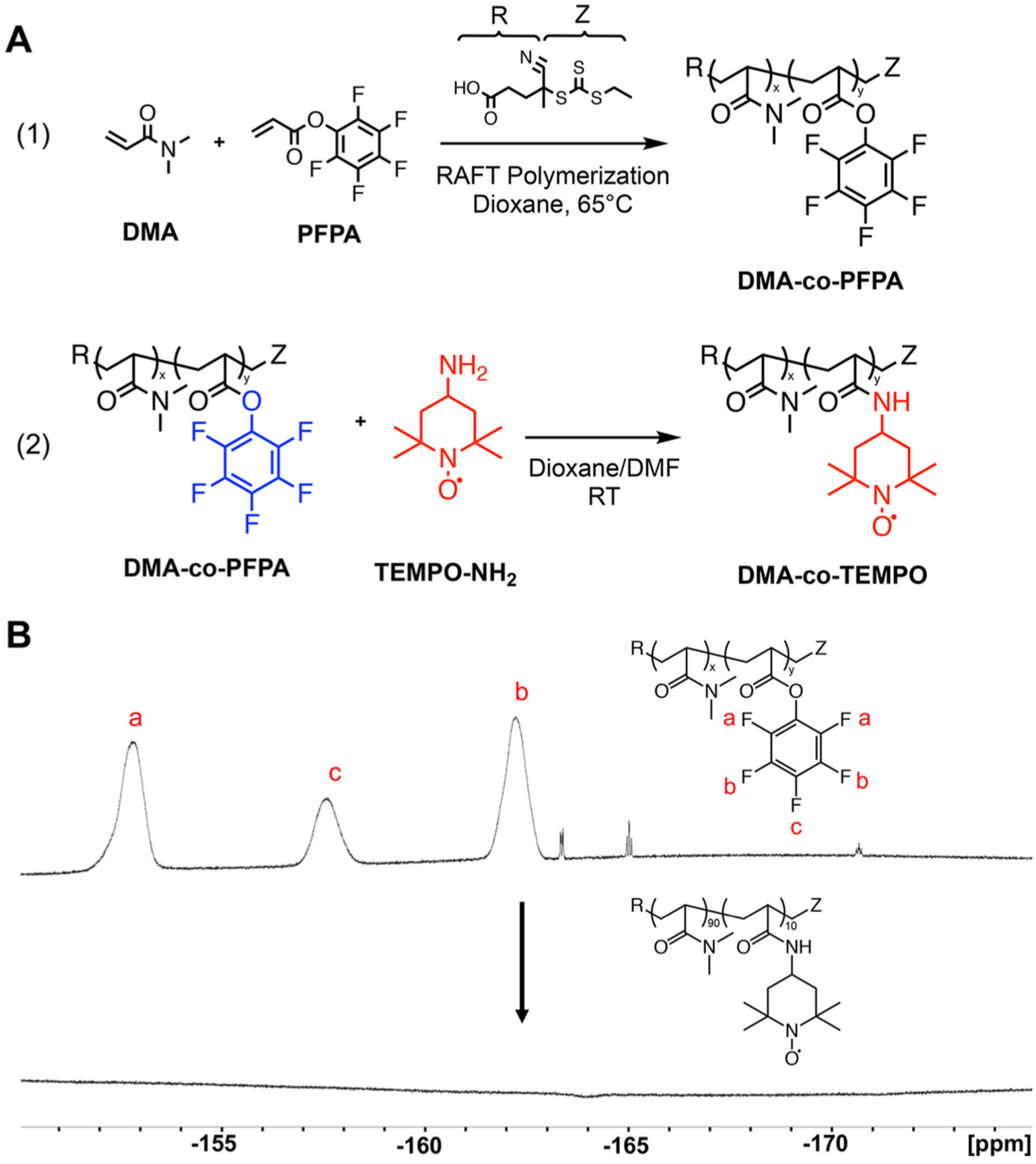


**Figure 1.**

RAFT polymerization and post-polymerization conjugation allows for facile and precise control of DMA-*co*-TEMPO copolymer synthesis. (A) Two-step synthesis scheme of polymers by (1) RAFT polymerization of DMA and PFPA and (2) post-polymerization substitution of TEMPO-amine for PFPA. (B) $^{19}$F NMR confirming removal of PFPA units on the final polymer.

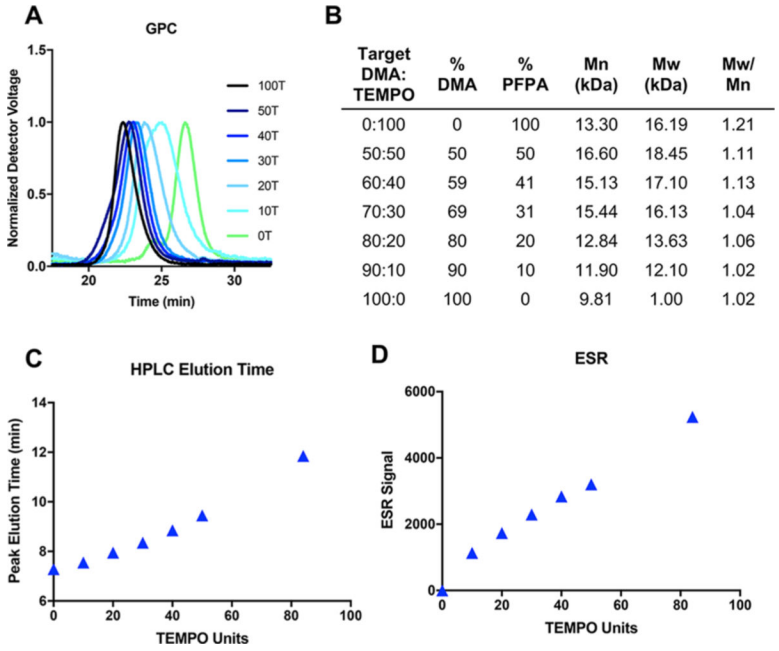


| Target DMA: TEMPO | % DMA | % PFPA | Mn (kDa) | Mw (kDa) | Mw/ Mn |
|---|---|---|---|---|---|
| 0:100 | 0 | 100 | 13.30 | 16.19 | 1.21 |
| 50:50 | 50 | 50 | 16.60 | 18.45 | 1.11 |
| 60:40 | 59 | 41 | 15.13 | 17.10 | 1.13 |
| 70:30 | 69 | 31 | 15.44 | 16.13 | 1.04 |
| 80:20 | 80 | 20 | 12.84 | 13.63 | 1.06 |
| 90:10 | 90 | 10 | 11.90 | 12.10 | 1.02 |
| 100:0 | 100 | 0 | 9.81 | 1.00 | 1.02 |

**Figure 2.**

DMA-*co*-TEMPO copolymer library represents a range of tunable molecular weights, hydrophobicities, and radical scavenging potentials. (A) Light scattering detector traces from GPC indicate monodisperse populations with increasing molecular weight as TEMPO content increases. (B) Table of characterization of DMA and PFPA composition of the parent copolymers, $M_n$ and $M_w$ of final polymers, and polydispersity of final polymers. (C) Reverse phase HPLC characterization shows that relative polymer hydrophobicity increases with increasing TEMPO content. (D) ESR characterization of copolymer radical content demonstrates active TEMPO conjugated in controllable density to the polymer backbone.

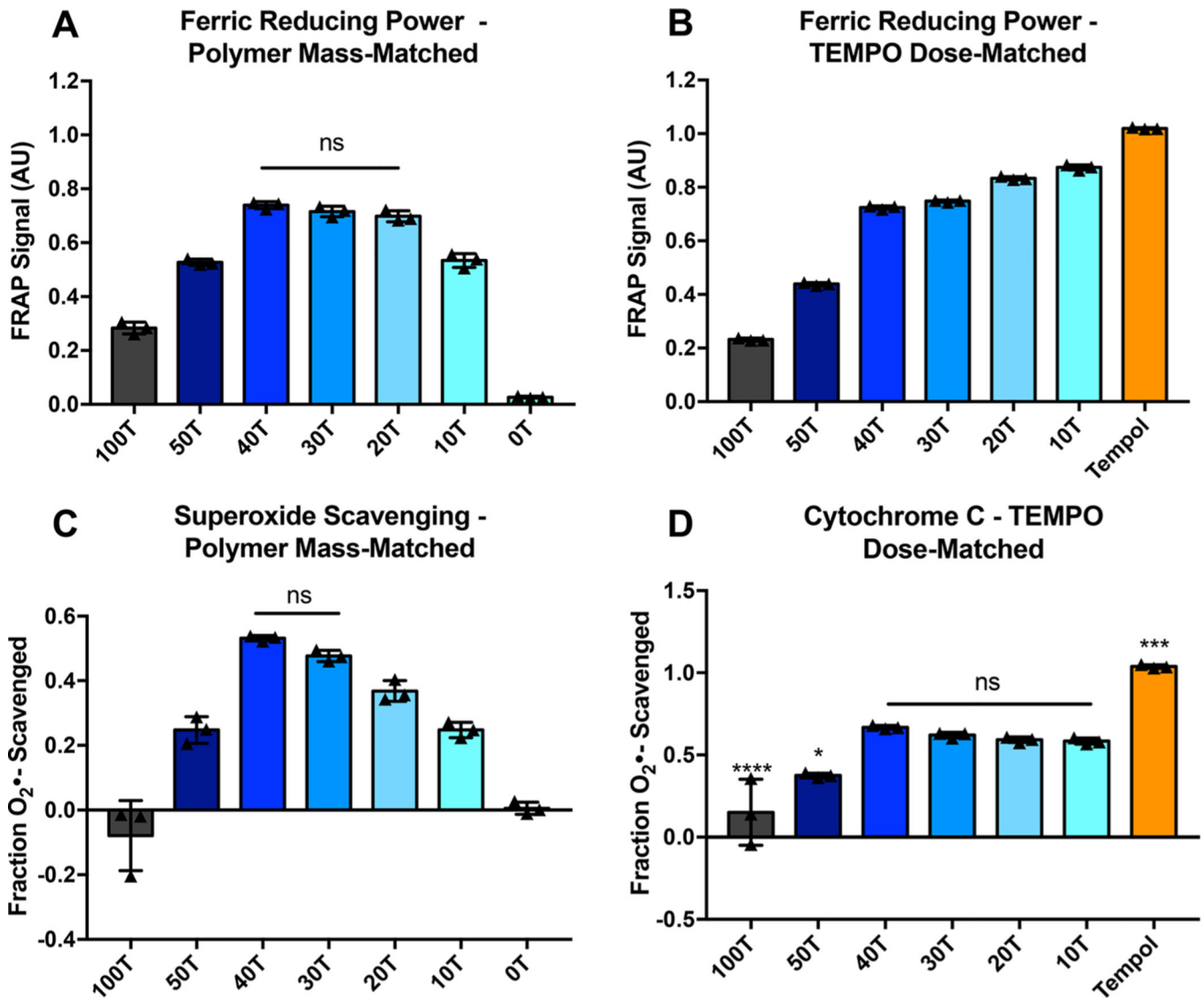


**Figure 3.**

Cell-free assays demonstrate that radical activity is optimal at a 30–40% TEMPO conjugation. (A and B) Ferric reducing power of library for polymer mass-matched (A, 0.2 mg/mL) and TEMPO dose-matched (B, 170 $\mu$M) scenarios. Polymers were dissolved or suspended in water and incubated with the FRAP reagent to measure general reducing power. (C and D) $O_2^{\bullet-}$ scavenging for polymer mass-matched (C, 0.2 mg/mL) and TEMPO dose-matched (D, 170 $\mu$M) scenarios. Polymers were dissolved or suspended in PBS and incubated with hypoxanthine/xanthine oxidase + cytochrome C to measure $O_2^{\bullet-}$ scavenging. ns = not significantly different. * = significantly different from 10% to 40% TEMPO polymers. *$p < 0.05$, ***$p < 0.001$, ****$p < 0.0001$.

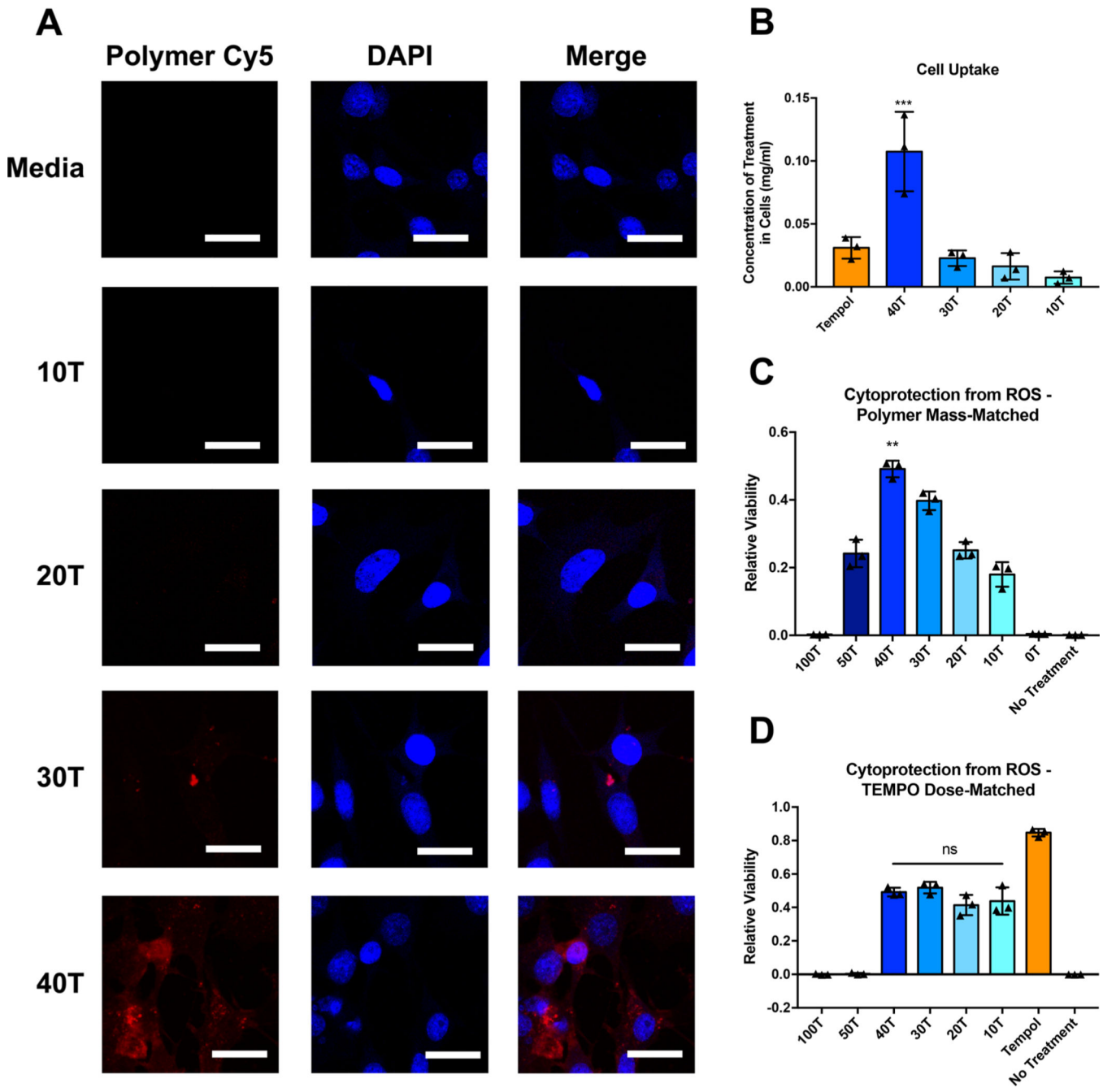


**Figure 4.**

DMA-*co*-TEMPO copolymers are differentially internalized by ATDC5 cells and protect them from SIN-1-induced cell death. (A) Cell uptake of Cy5-labeled polymers observed by fluorescent microscopy after 24 h treatment. 40T exhibits the highest Cy5 signal. Scale bar = 25 $\mu$m. (B) Cell uptake results were confirmed by ESR. Signal was normalized to inherent TEMPO signal to control for variable backbone density of TEMPO and allow for direct comparison between treatments. (C and D) Cytoprotection from ROS-induced cell death in polymer mass-matched (C, 0.2 mg/mL) and TEMPO dose-matched (D, 170 $\mu$M) scenarios. Cells were treated with 1 mM SIN-1 ± treatments for 24 h, and viability was normalized to

cells in normal media. * = significantly different from all other groups. ** $p < 0.005$, ns = not significantly different.

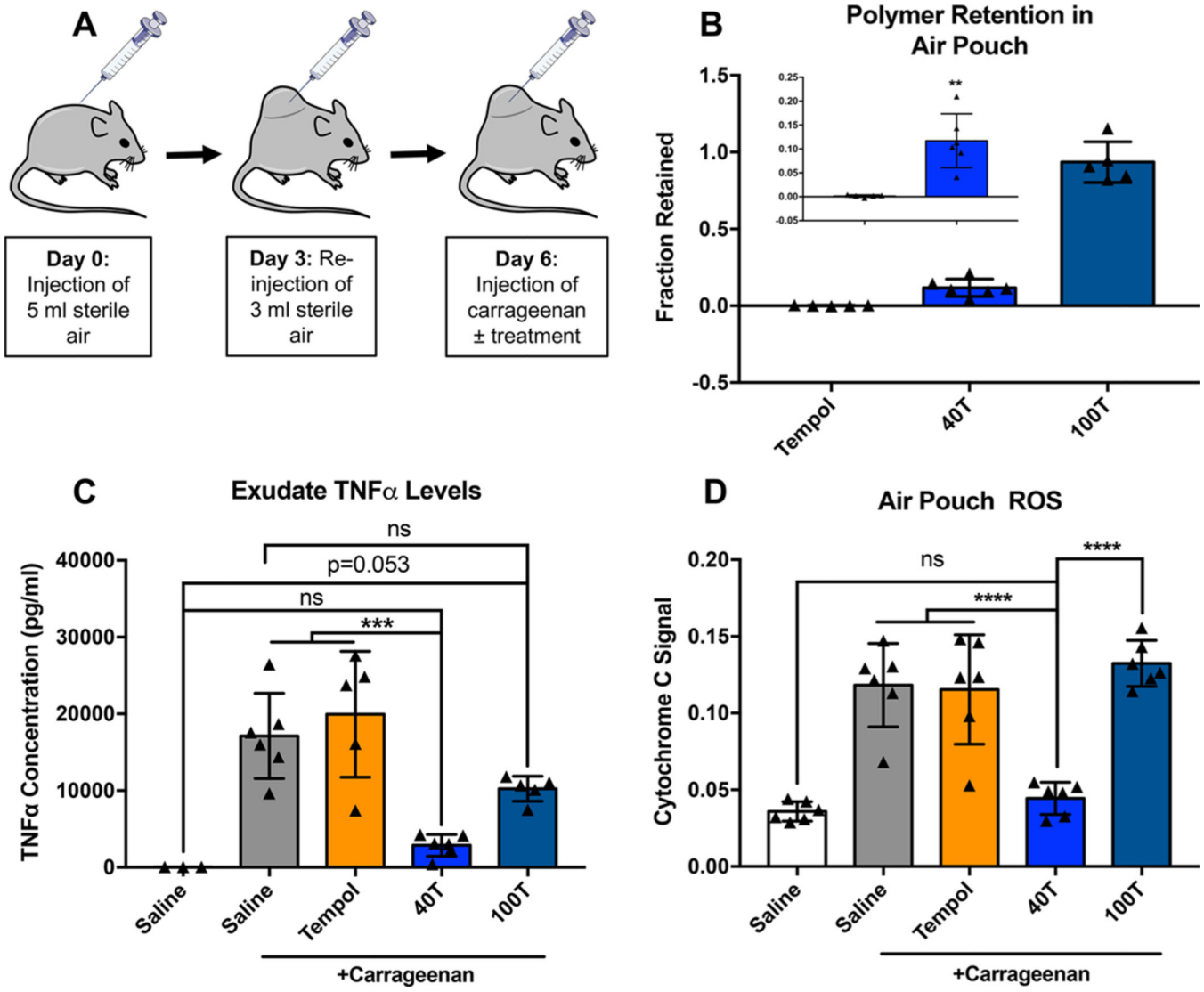


**Figure 5.**

40T outperforms free Tempol and 100T in a local inflammation model. (A) Experimental setup: mice were injected with 5 mL air to establish the air pouch, which was reinjected with air 3 days later. Inflammatory carrageenan ± treatments was injected on day 6. All treatments were matched at a TEMPO dose of 8.48 $\mu$mol. (B) Polymer retention in exudate 6 h after carrageenan treatment. Inset = 40T copolymer compared with Tempol. Cell-laden exudate was collected, and polymer content was measured by ESR. (C) TNF-a levels in exudate measured by ELISA after separation of exudate fluid from exudate cells. (D) ROS levels in air pouch exudate measured by cytochrome C. Fresh exudate was combined with cytochrome C, and absorbance was measured on a plate reader. $^{**}p < 0.005$, $^{***}p < 0.001$, $^{****}p < 0.0001$, ns = not significantly different.

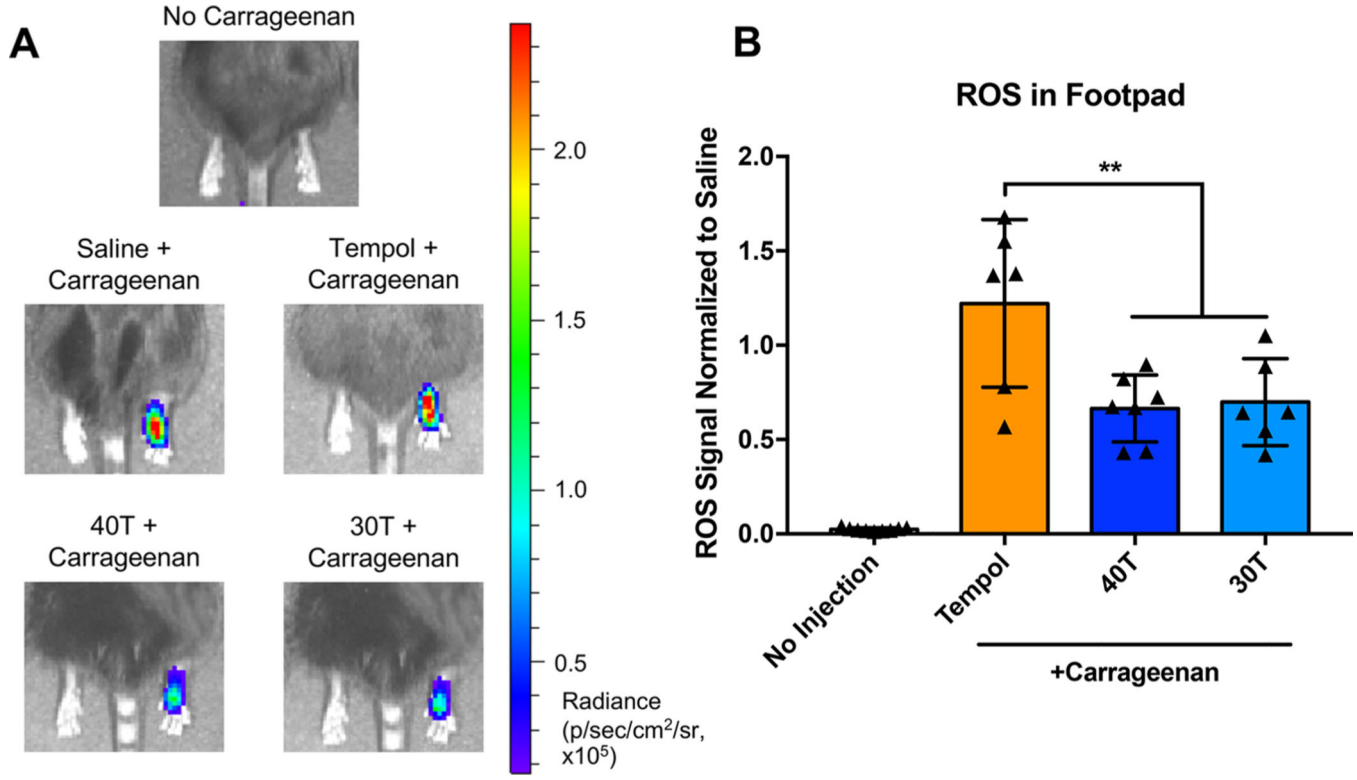


**Figure 6.**

TEMPO polymerization improves ROS scavenging with systemic administration in a footpad model of inflammation. (A) Representative IVIS images of luminol signal in C57/Bl6 mouse paws after carrageenan injection and polymer treatment. Carrageenan inflammation was allowed to establish for 6 h, followed by i.v. injection of treatments. All treatments were matched at a TEMPO dose of 377 nmol. (B) Luminol signal normalized to carrageenan + saline treated group. $^{**}p < 0.005$.